Feedback Control of High-Lift State
for A Low-Aspect-Ratio Wing

Kunihiko Taira[*] and Clarence W. Rowley[†]

Princeton University, Princeton, New Jersey, 08536

Tim Colonius[‡]

California Institute of Technology, Pasadena, California, 91125

The objective of this study is to employ feedback control to maximize time-average lift on a low-aspect-ratio wing by directly modifying the three-dimensional dynamics of the wake vortices. Flow control around such wing at post-stall angles of attack is numerically investigated at a low Reynolds number of 300 with blowing along the trailing edge. Motivated by the existence of time-periodic high-lift states under open-loop control with periodic excitation, the extremum seeking algorithm is considered for designing feedback control to lock the flow onto such high-lift states. Preliminary results are presented where the close-loop control is able to seek the optimal actuation frequency and yield high lift.

Introduction

Unsteady separated flows are ubiquitous in biological flight and swimming. The understanding of vortex dynamics around low-aspect-ratio wings or foils is expected to aid further enhancement of the aerodynamic performance and explore novel flight mechanism of micro air vehicles (MAVs) [1, 2]. We place emphasis on the use of unsteadiness and the three-dimensionality of the flow in this study, and investigate separated flows around wings at post-stall angles of attack, sharing similar parameter space with small insects in terms of the Reynolds number and the aspect ratio of the wings. The objective here is to utilize feedback flow control to enhance lift on a translational wing by positioning the leading-edge vortex closer to the top surface of the wing, a mechanism often used in flapping flights for added lift [3–5].

A number of studies have been performed in the past to investigate the use of flow control to enhance aerodynamic performance of airfoils at high angles of attack. In particular, the use of periodic excitation has been considered by Seifert *et al.* [6, 7], Greenblatt *et al.* [8], and Amitay and Glezer [9] for delaying airfoil stall. The difference between these studies and the current investigation is the use of three-dimensionality of vortex dynamics for possible aerodynamic benefit. This is especially important for low-aspect-ratio wings whose tip effects affect the flow separation physics.

Based on our previous studies in understanding the three-dimensional unsteady vortex dynamics around purely translating low-aspect-ratio wings [10], we have recently considered the application of steady [11] and periodic [12] blowing for flow control. Unlike most other investigations, the objective was *not* to reattach the flow or delay separation. The three-dimensional dynamics of the wake vortices was modified to effectively increase lift on low-aspect-ratio wings. It was also observed that when the open-loop actuation frequency is slightly lower or higher than the natural shedding frequency, the vortex shedding locks onto a *time-periodic high-lift state* that enhances lift by more than a double compared to the unactuated case.

Motivated by the existence of such state, we consider the use of feedback control to stabilize lift at the optimal actuation frequencies. The closed-loop controller is designed using the extremum seeking algorithm [13] and demonstrated to find the optimal forcing frequency to enhance lift.

---

[*]Postdoctoral Research Associate, Department of Mechanical and Aerospace Engineering. Member AIAA.

[†]Associate Professor, Department of Mechanical and Aerospace Engineering. Associate Fellow AIAA.

[‡]Professor, Division of Engineering and Applied Science. Associate Fellow AIAA

Simulation Approach

Spatial and Temporal Discretization

Separated flows around low-aspect-ratio rectangular wings are simulated with the immersed boundary projection method [14, 15]. The spatial domain is discretized with a Cartesian grid and the wing is represented by a collection of Lagrangian points where a regularized boundary forces is added to the right-hand-side of the incompressible Navier-Stokes equations to satisfy the no-slip condition. The method is based on the second-order staggered-grid finite-volume formulation with the Crank-Nicolson and the second-order Adams-Bashforth schemes for the viscous and convective terms, respectively. For details on the computational method, we refer the readers to Refs. [14] and [15].

Simulations are performed in an sufficiently large box. Grid stretching is applied away from the wing and uniform flow of $(U_\infty, 0, 0)$ is applied at the computational boundary except for at the outflow boundary, where a convective boundary condition $\partial \mathbf{u}/\partial t + U_\infty \partial \mathbf{u}/\partial x = 0$ is specified. Typical grid resolution of $150 \times 66 \times 156$ is used and was verified to be sufficiently converged [10]. The wing is infinitely thin in the limit of $\Delta x \to 0$ but, with finite resolution of order Δx in the computation.

The simulations are started by instantaneously materializing the wing at $t = 0^+$ with its center at the origin in an initially uniform flow. In this paper, the temporal variable t is taken to be the non-dimensional convective time based on the freestream velocity and the wing chord. The time step is chosen such that $U_\infty \Delta t / \Delta x \leq 0.5$. These choice of parameters for the simulations are based on prior validations in flow physics [10] and open-loop control studies [11, 12].

To study laminar separation behind the low-aspect-ratio wing at post-stall angles of attack, the Reynolds number is selected to be $Re \equiv U_\infty c/\nu = 300$. The lift and drag coefficients are reported as $C_L \equiv F_y/\frac{1}{2}\rho U_\infty^2 bc$ and $C_D \equiv F_x/\frac{1}{2}\rho U_\infty^2 bc$, respectively, where b is the wing span. The aspect ratio of the rectangular wing is defined as $AR \equiv b^2/bc = b/c$.

Actuator Model

The current actuator is a sinusoidal external force added to the momentum equation, mimicking the zero-net-mass-flux actuator (synthetic jet). This actuator is selected for this study as it has been found to be more effective in other flow control studies compared to steady blowing [6, 16]. The benefit of using this type of actuator is also observed in the present study through the synthetic jet model. In the simulation, the amplitude of the actuator is sinusoidal in time and is defined in the following fashion:

$$\mathbf{f}_{\mathrm{act}} = \hat{\mathbf{f}}_{\mathrm{act}} \left[1 - \cos(\omega_{\mathrm{act}} t)\right]/2, \tag{1}$$

where the blowing direction and magnitude is specified with $\hat{\mathbf{f}}_{\mathrm{act}}$. While the actuation frequency ω_{act} is constant in the open-loop studies, this frequency is later changed to be time-varying based on a feedback law in the closed-loop cases.

For all cases presented in the current paper, actuation is introduced along the entire trailing edge with momentum injection in the downstream direction parallel to the wing surface. This control setup was realized to be the most effective choice among the various combination of actuator locations and directions examined in a previous steady forcing study at $Re = 300$ [11]. The actuator is placed three grid cells above the top surface of the wing to avoid numerical interference between the actuator and the immersed boundary force. A schematic of the actuator setup is presented in Fig. 1.
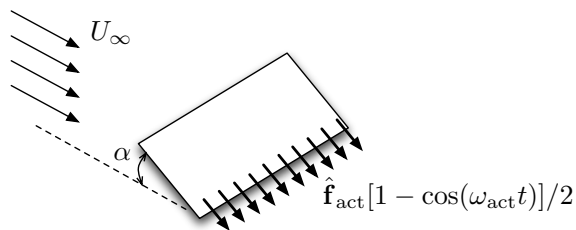

Figure 1. Setup of the trailing-edge actuation.

In the following sections, we report the control effort with two non-dimensional parameters, namely:

$$\overline{C}_\mu \equiv \frac{\rho \overline{u}_{\text{act}}^2 \sigma b}{\frac{1}{2} U_\infty^2 bc} \qquad \text{(steady momentum coefficient)} \qquad (2)$$

$$\langle C_\mu \rangle \equiv \frac{\rho \langle u_{\text{act}} \rangle^2 \sigma b}{\frac{1}{2} U_\infty^2 bc} \qquad \text{(oscillatory momentum coefficient)} \qquad (3)$$

where the quantities with over bar and $\langle \ \rangle$ represent time-average and root-mean-square values, respectively. The slot width σ is set to be the effective width of the regularized delta function [17] that is used to represent the actuator and is $\sigma/c = \Delta x/c = 0.04$. We also note that in the present model, there is no mass injection to the fluid.

Separated Flow

When a wing at a post-stall angle of attack undergoes an impulsive translation, the wing experiences a large lift which eventually decays to the steady value at large time. At high angles of attack, flow separates and creates a leading-edge vortex above the wing, whose low-pressure core provides increased lift. This phenomena is similar to dynamic stall observed for blades undergoing a rapid increase in the angle of attack. Compared with the early time, the wake structures are different at large time, especially the leading-edge vortices that form further away from the top surface, resulting in the reduction of lift. Here, we consider the use of actuation to modify the dynamics of the wake in order to increase lift to the level that is achieved early in time. Our objective is not to delay stall or reattach the flow, but to increase lift by modifying the dynamics of the wake vortices behind the low-aspect-ratio wings at post-stall angles of attack.

Without control, separated flows around rectangular wings at post-stall angles of attack exhibit steady separation, periodic shedding, or aperiodic shedding. For example, at $Re = 300$ and $AR = 2$, the flow is steady for $0° \lesssim \alpha \lesssim 19°$, unsteady with periodic shedding for $19° \lesssim \alpha \lesssim 28°$, and unsteady with aperiodic shedding for $28° \lesssim \alpha$. The periodic shedding occurs at a distinct frequency of

$$St \equiv f_n c \sin \alpha / U_\infty \approx 0.12, \qquad (4)$$

while for higher angles of attack, shedding no longer occurs at this single frequency. For details on the shedding behavior and the stability of the wake, see Ref. [10]. This relation (shedding frequency) will be extended for angles of attack outside of the periodic states in actuating the flow.

Open-Loop Control

Application of Steady Forcing

First, let us consider the influence of steady forcing applied along the trailing edge in the downstream direction. This control setup is able to convect the trailing-edge vortex sheet away from the wing without much interaction with the leading-edge vortex. While the sheet is convected, it is rolled into the tip vortices, which strengthens the downward-induced velocity upon the leading-edge vortex. Hence the low pressure vortex core is positioned closer to the top surface of the wing, providing enhanced lift (see also Fig. 7 in Ref [11]). The wake structures are visualized for cases with (a) no control and (b) steady blowing in Fig. 2 with $\overline{C}_\mu = 1.0\%$ and $\langle C_\mu \rangle = 0$. As it is mentioned above, the stronger and longer formation of tip vortices is visible in the figure.

For a momentum coefficient of $0.5\% \leq \overline{C}_\mu \leq 1.0\%$, lift enhancement of 22 to 143% is observed for wings with various aspect ratios from 1 to 4, at angles of attack up to 40°. Since the focus of the present paper is in open and closed-loop control with sinusoidal excitation, readers are referred to Ref. [11] for further discussion on the steady forcing results.

Application of Periodic Excitation

We consider the application of periodic forcing around a wing of $AR = 2$ at $\alpha = 30°$. While the current case results in aperiodic shedding in uncontrolled flow, the excitation frequency is selected by extrapolating the natural shedding frequency for the periodic shedding case (Eq. 4), *i.e.*, $\omega_n \equiv 2\pi St U_\infty / c \sin \alpha$.
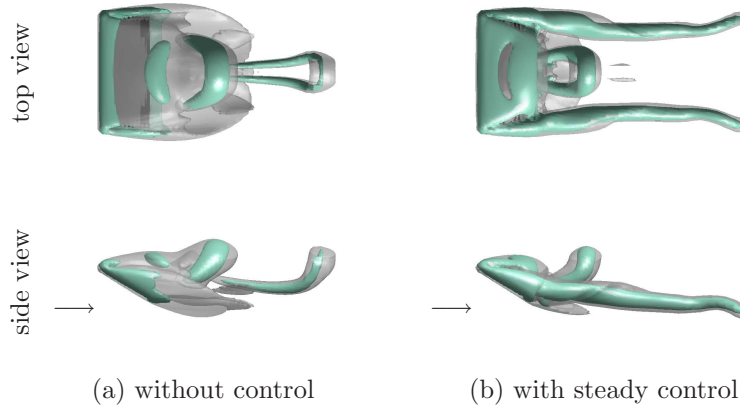
Figure 2. Snapshots of the wake structures for $AR = 2$, $Re = 300$, and $\alpha = 30°$ with and without control. Shown are the iso-surfaces of $\|\boldsymbol{\omega}\|_2 = 3$ (light gray) and $Q = 2.5$ (dark gray). Arrows indicate the flow direction.

To demonstrate the advantage of using periodic excitation, we compare cases with periodic forcing of $\overline{C}_\mu = 0.5\%$ and $\langle C_\mu \rangle = 0.25\%$ with steady forcing case. The actuation frequency is set to the natural shedding frequency (i.e., $\omega_{\rm act}/\omega_n = 1$). The lift coefficient is shown in Fig. 3, along with cases without control and with steady blowing at $\overline{C}_\mu = 0.5\%$ and 1.0%. It can be noted that the periodic forcing case can achieve significant increase in lift from the uncontrolled case, with less momentum injection compared to those with steady blowing. Hence in what follows reduced actuation effort with $\overline{C}_\mu = 0.5\%$ and $\langle C_\mu \rangle = 0.25\%$ is always used. We note in passing that, with control, drag is not increased as much as the lift coefficient in comparison to the unactuated case.
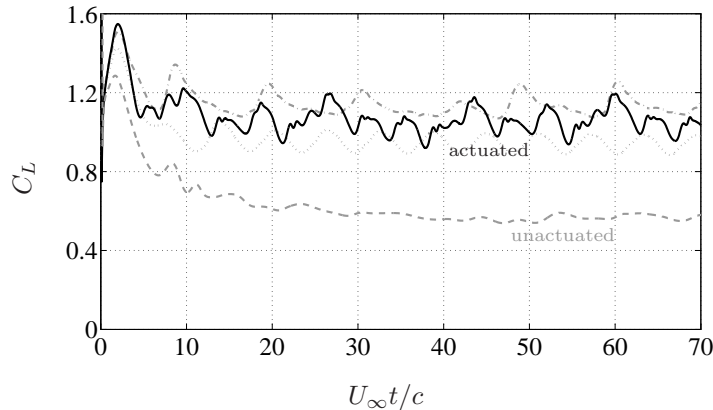

Figure 3. Lift force on a wing of $AR = 2$ at $\alpha = 30°$ with steady (⋯⋯⋯⋯ $\overline{C}_\mu = 0.5\%$, - - - - - $\overline{C}_\mu = 1.0\%$) and periodic forcing (—— $\overline{C}_\mu = 0.5\%$, $\langle C_\mu \rangle = 0.25\%$) along the trailing edge. The unactuated case is also shown (- - -).

Influence of Actuation Frequency

Let us next consider the effect of the actuation frequency on the behavior of lift. For flows excited with frequency above ω_n, high frequency modulation generated by the forcing frequency is observed. Shown in Fig. 4(a) is the case where $\omega_{\rm act}/\omega_n = 4$. The trend in terms of the average the lift is similar to the case where the blowing frequency is ω_n, but with larger oscillation amplitude.

An interesting case is observed when we choose to blow the trailing-edge vortex sheet at a frequency slightly less than ω_n as shown in Fig. 4(b). For $\omega_{\rm act}/\omega_n = 0.75$, the minimum value of lift is also enhanced,
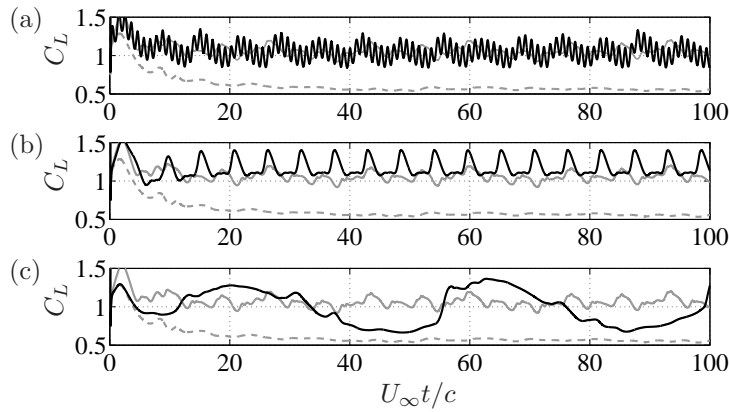
Figure 4. Time trace of lift (——) for (a) $\omega_{\mathrm{act}}/\omega_n = 4$, (b) $\omega_{\mathrm{act}}/\omega_n = 0.75$, and (c) $\omega_{\mathrm{act}}/\omega_n = 0.1$ with the unactuated and $\omega_{\mathrm{act}}/\omega_n = 1$ results superposed as (- - -) and (——), respectively.

shifting the time-average lift to the largest value out of all frequencies considered in this study. The shedding locks onto a *time-periodic high-lift state*. This agrees with the findings of Seifert *et al.* [6] that notes the optimal behavior occurs when $\omega_{\mathrm{act}}/\omega_n \approx 1$. As we examine the lift trace, we notice that the there is regular shedding. The difference between this case with other cases is that the roll up of trailing-edge vortex sheet into the tip vortices (strengthening mechanism) and the formation of the leading-edge vortices are in synchronization.

For forcing frequency of $\omega_{\mathrm{act}}/\omega_n \lesssim 0.5$, we observe significant variation in lift over time with a decrease in the minimum lift close to the level of the unactuated case. See for example, Fig. 4(c), where $\omega_{\mathrm{act}}/\omega_n = 0.1$. The tip vortices convect away from the wing in between the occurrence of blowing, resulting in the loss of the tip vortices' columnar structures and their corresponding downward-induced velocity. The key here is to avoid decrease in lift or its large fluctuation over time, by actuating with a time scale less than the time required for the tip vortices to lose their structures.
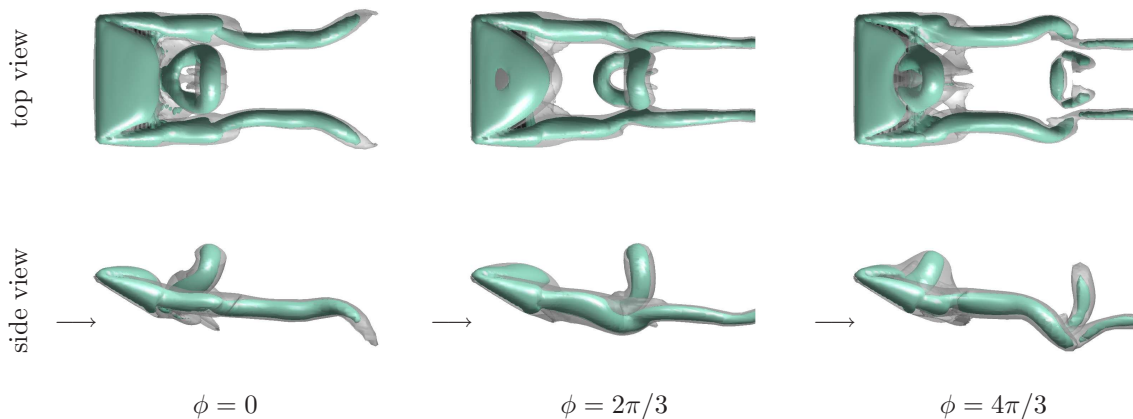
Figure 5. Snapshots of the periodically time-varying wake structures shown for every one-third phase interval for the controlled case with $\omega_{\mathrm{act}}/\omega_n = 0.75$. Shown are the iso-surfaces of $\|\boldsymbol{\omega}\|_2 = 3$ (light gray) and $Q = 2.5$. Arrows indicate the flow direction.

Let us revisit the actuation frequency of $\omega_{\mathrm{act}}/\omega_n = 0.75$. The flow is time-periodic, as visualized in Fig. 5. The snapshots are sampled at three equally spaced phases ($\phi = 0$, $2\pi/3$, and $4\pi/3$) over a shedding cycle. The first snapshot at $\phi = 0$ is selected to be at the time of maximum lift with the leading-edge vortex is covering the whole top surface of the wing. As time progresses to $\phi = 2\pi/3$, the tip vortices start to thin out near the rear corners of the wing with reduced blowing. By the time of $\phi = 4\pi/3$, the tip vortices cease

to roll up the trailing-edge vortex sheet and hence reduces the downward induced velocity applied on the leading-edge vortex. Around this time, the leading-edge vortex sheds from wing, interestingly in a cleanly shaped vortex ring (clearly visible with the visualization at $\phi = 2\pi/3$). Due to this synchronization, the flow *locks onto a high-lift state* by keeping the low-pressure core of the leading-edge vortices as close as possible to the top surface in between their detachment.
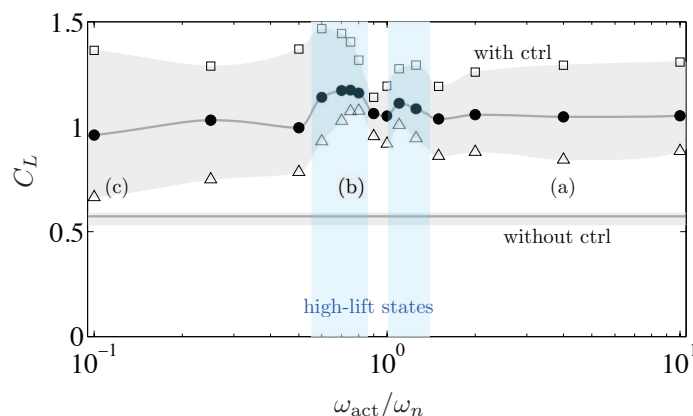
Figure 6. Variation in lift for different actuation frequencies for $AR = 2$ and $\alpha = 30°$ shown on the left. Time-average lift coefficients ($\bullet$) are plotted their maxima ($\square$) and minima ($\triangle$). The horizontal line (——) denotes the average lift for the unactuated case bounded by its minimum and maximum illustrated by the shaded box.

Next, the actuation frequency is varied from 0.1 to 10 times the natural periodic shedding frequency, ω_n, around an $AR = 2$ wing at $\alpha = 30°$. The forcing inputs of $\overline{C}_\mu = 0.5\%$ and $\langle C_\mu \rangle = 0.25\%$ are selected as in the previous examples. In Fig. 6, the variations in time-average lift are shown for different forcing frequencies. The bars and the shade represent the amplitude of oscillation in the lift coefficient. Also illustrated by the horizontal line is the lift for the uncontrolled case. The lift is enhanced with periodic excitation for all considered frequencies.

Highlighted in Fig. 6 are the two desirable ranges of frequencies where the time-average lift are higher than those other forcing frequencies (i.e., $\omega_{\text{act}}/\omega_n \approx 0.75$ and 1.1). From preliminary investigation, it is suspected that these two different regions corresponds different mechanisms of lock-on (perhaps related to period-1 and 2). The goal in the next section is to lock the flow within the bands of optimal frequencies for high lift without prior knowledge of lift response to actuation frequencies.

Closed-Loop Control

Extremum Seeking Control

The extremum seeking control [13, 18, 19] adds a perturbation ($a \sin \omega t$) to the system near a maximum operating point, which in this case corresponds to the maximum time-average lift achieved for a range of actuation frequency. A diagram of the extremum seeking algorithm is shown by the lower part of Fig. 7. The resulting output signal is put through a high-pass filter to remove the DC component and is demodulated with the input perturbation. This demodulated function can then be passed through an integrator as an approximate gradient update to improve the guess of the maximum operating point.

The advantage of this method is that the dynamics of the flow need not be characterized and can be treated as a nonlinear black box. Hence this approach seems as a promising path to stabilize the flow about its high-lift state. The only concern in designing this controller is the ratio of speeds at which the flow reacts and the controller updates its optimal point of operation. If the nonlinearity changes the flow field in a shorter time than that for the controller to take its effect, the algorithm can be ineffective or in some instances the flow can lock onto a different cycle from what is observed in the open-loop control cases.

In the current study, we aim to lock the shedding to $\omega_{\text{act}}/\omega_n \approx 0.75$ or 1.1 that corresponds to frequency at which the time-average lift is at its local maximum (see Fig. 6). The immersed boundary projection method will take the control input of actuation frequency and provide the lift force on the wing as the output. The lift is passed through a time-averaging routine prior to entering the extremum seeking algorithm, as depicted by the top portion of Fig. 7.
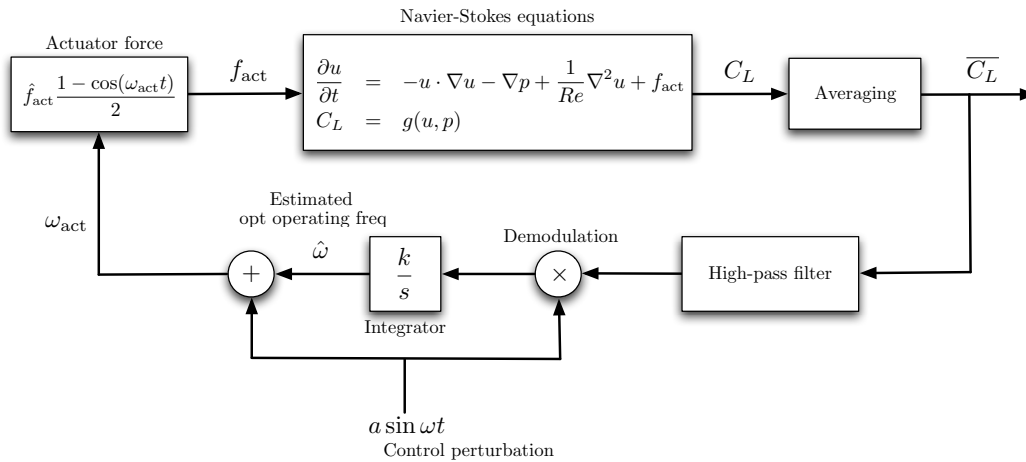
Figure 7. Setup of extremum seeking control to achieve maximum average lift.

The control parameters to be chosen for the extremum seeking algorithm are a and ω for the control perturbation, the integral gain k, and the cutoff frequency Ω_H for the high-pass filter. The perturbation $a\sin(\omega t)$ is selected such that it is small compared to the variable to control (ω_{act}) and is slowly varying compared to the main physics of interest (shedding). Hence we select the parameters as:

$$a \ll \omega_{\mathrm{act}} \Rightarrow a = 0.0375 \qquad \text{and} \qquad \omega \ll \omega_n \Rightarrow \omega = 0.15.$$

The integral gain k is set to be 0.5 (near unity) and the cutoff frequency Ω_H is set to be equal to ω inside the 3rd order high-pass Butterworth filter.

We start the simulation with feedback control using an initial condition near the optimal forcing frequency at some large time t_0. Preliminary findings for the time evolution of actuation frequency and time-average lift are shown in Fig. 8. The extremum seeking algorithm quickly locks the estimated optimal operating frequency to $\hat{\omega}/\omega_n = 0.8$, near the optimal frequency in the open-loop control case (≈ 0.75).
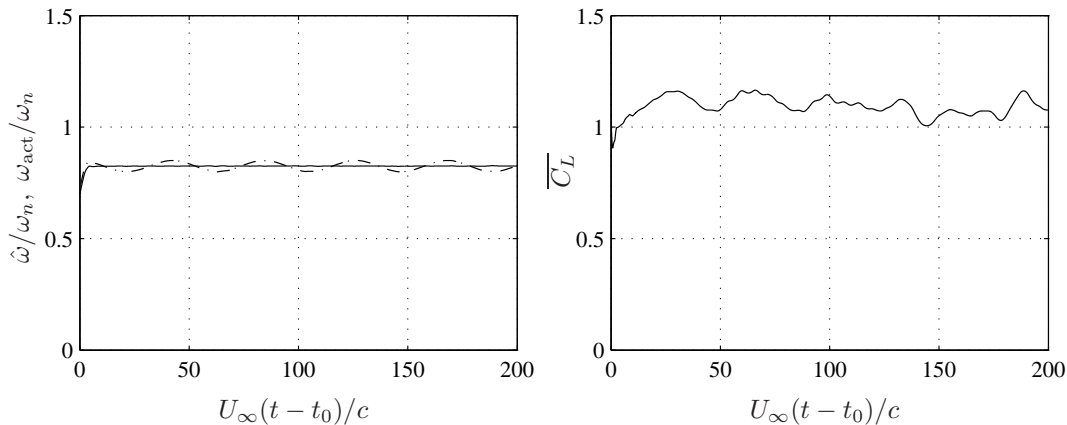

Figure 8. Preliminary results of actuation frequency locking on near a local optimum frequency. Shown on the left are the estimated optimal operating frequency $\hat{\omega}$ and the actuation frequency ω_{act}, respectively with (——) and (-----). The right plot illustrates the average lift coefficient over time. Longer duration of simulation is required for final assessment.

It can be noticed that the actuation frequency seems to converge faster to the optimal actuation frequencies, compared to the time-average lift. This can be a result of how the lift averaging is performed. In the present method, we simply compute the average over a few periods; this can be replaced by a low-pass filter instead. The performance and the time lag introduced by the choice of averaging may have affected how soon the time-average lift achieves steady state.

The lift trace with feedback control is shown on Fig. 9 starting from the time the closed-loop control is turned on. The results show that the actuation frequency stays slightly above the optimal open-loop forcing

American Institute of Aeronautics and Astronautics Paper 2010-357

frequency (≈ 0.75). Unlike the open-loop case, the close-loop actuation is not able to lock onto a periodic flow and exhibit time variation in the average lift (Fig. 8). Nonetheless, we achieve lift enhancement of approximately double of the unactuated case.
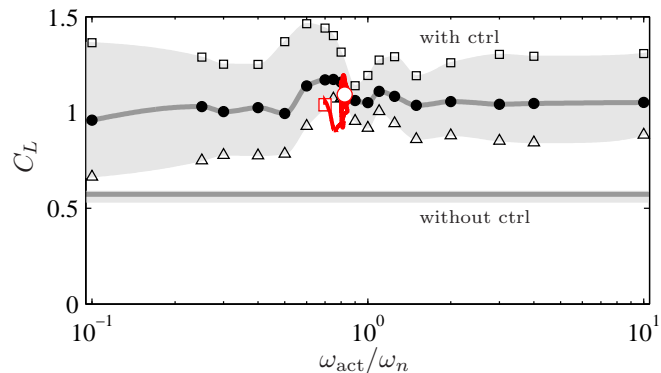
Figure 9. The lift trace with feedback control plotted against its actuation frequency, superposed on Fig. 6. The initial condition and the steady time average value are represented by □ and ○, respectively.

The vortex dynamics behind low-aspct-ratio wings appears to be sensitive to temporal changes to the forcing frequency, perhaps making the flow unable to lock onto a periodic cycle. Thus, it may be useful to consider a smaller magnitude a of perturbation, letting the feedback to slowly search for optimal operation point.

The extremum seeking algorithm here does not take into account the phase difference between the controller and the output signal. Since there most likely is time delay associate with vortex formation and lag from averaging, the inclusion of a phase ϕ in the perturbation signal (i.e., $a\sin(\omega t + \phi)$) for demodulation may be necessary. In an analogous two-dimensional study [20], the phase in the forcing was found to be important in locking the flow to periodic high-lift states. Hence, it may be beneficial here to update the phase through feedback along with the forcing frequency or to relate the phase to the physical time scale associated with vortex dynamics in an approximate fashion.

Additional control designs are currently being investigated to understand the influence of each control parameter on the performance of the feedback controller. Computations are also undertaken to address whether the extremum seeking algorithm can reach a higher time-average lift than that in the shown preliminary result.

Summary

The post-stall flows around low-aspect-ratio wings at high angles of attack can be modified to achieve enhanced lift with the application of downstream blowing along the trailing edge. Open-loop actuation was examined for a range of actuation frequency and was observed that for $\omega_{\mathrm{act}}/\omega_n \approx 0.75$ and 1.1, the vortex shedding locks on to states that yield higher lift compared to other actuation frequencies.

We further consider the use of feedback control about the time-periodic high-lift states achieved with the open-loop control. The closed-loop control was designed using the extremum seeking algorithm, with the objective of locking the separated flows onto the high-lift states with the optimal forcing frequencies. Preliminary results indicate that separated flows can lock onto such optimal actuation frequencies to maximize lift. A case is presented that increases lift by approximately double with the forcing frequency locking onto $\omega_{\mathrm{act}}/\omega_n \approx 0.8$, which is near the optimal open-loop actuation frequency.

Acknowledgments

References

[1] Mueller, T. J., editor, *Fixed and flapping wing aerodynamics for micro air vehicle applications*, Vol. 195 of *Progress in Astronautics and Aeronautics*, AIAA, 2001.

[2] Pines, D. J. and Bohorquez, F., "Challenges facing future micro-air-vehicle development," *Journal of Aircraft*, Vol. 34(2), 2006, pp. 290–305.

[3] Ellington, C. P., van den Berg, C., Willmott, A. P., and Thomas, A. L. R., "Leading-edge vortices in insect flight," *Nature*, Vol. 384, 1996, pp. 626–630.

[4] Birch, J. M. and Dickinson, M. H., "Spanwise flow and the attachment of the leading-edge vortex on insect wings," *Nature*, Vol. 412, 2001, pp. 729–733.

[5] Birch, J. M., Dickson, W. B., and Dickinson, M. H., "Force production and flow structure of the leading edge vortex on flapping wings at high and low Reynolds numbers," *Journal of Experimental Biology*, Vol. 207, 2004, pp. 1063–1072.

[6] Seifert, A., Darabi, A., and Wygnanski, I., "Delay of airfoil stall by periodic excitation," *Journal of Aircraft*, Vol. 33(4), 1996, pp. 691–698.

[7] Seifert, A., Greenblatt, D., and Wygnanski, I. J., "Active separation control: an overview of Reynolds and Mach numbers effects," *Aerospace Science and Technology*, Vol. 8, 2004, pp. 569–582.

[8] Greenblatt, D., Neuburger, D., and Wygnanski, I., "Dynamic stall control by intermittent periodic excitation," *Journal of Aircraft*, Vol. 38(1), 2001, pp. 188–190.

[9] Amitay, M. and Glezer, A., "Role of actuation frequency in controlled flow reattachment over a stalled airfoil," *AIAA Journal*, Vol. 40(2), 2002, pp. 209–216.

[10] Taira, K. and Colonius, T., "Three-dimensional separated flows around low-aspect-ratio flat plates," *Journal of Fluid Mechanics*, Vol. 623, 2009, pp. 187–207.

[11] Taira, K. and Colonius, T., "Effect of tip vortices in low-Reynolds-number poststall flow control," *AIAA Journal*, Vol. 47(3), 2009, pp. 749–756.

[12] Taira, K., Rowley, C. W., Colonius, T., and Williams, D. R., "Lift enhancement for low-aspect-ratio wings with periodic excitation," *AIAA Journal*, 2009 in review.

[13] Ariyur, K. B. and Krstić, M., *Real-time optimization by extremum-seeking control*, Wiley, 2003.

[14] Taira, K. and Colonius, T., "The immersed boundary method: a projection approach," *Journal of Computational Physics*, Vol. 225, 2007, pp. 2118–2137.

[15] Colonius, T. and Taira, K., "A fast immersed boundary method using a nullspace approach and multi-domain far-field boundary conditions," *Computer Methods in Applied Mechanics and Engineering*, Vol. 197, 2008, pp. 2131–2146.

[16] Glezer, A. and Amitay, M., "Synthetic jets," *Annual Review of Fluid Mechanics*, Vol. 34, 2002, pp. 503–529.

[17] Roma, A. M., Peskin, C. S., and Berger, M. J., "An adaptive version of the immersed boundary method," *Journal of Computational Physics*, Vol. 153, 1999, pp. 509–534.

[18] Krstić, M. and Wang, H.-H., "Stability of extremum seeking feedback for general nonlinear dynamic systems," *Automatica*, Vol. 36, 2000, pp. 595–601.

[19] Wang, H.-H. and Krstić, M., "Extremum seeking for limit cycle minimization," *IEEE Transactions on Automatic Control*, Vol. 45 (12), 2000, pp. 2432–2437.

[20] Joe, W. T., Taira, K., Colonius, T., MacMynowski, D. G., and Tadmor, G., "Closed-loop control of vortex shedding on a two-dimensional flat-plate airfoil at a low Reynolds number," 2008, *AIAA Paper 2008-634*.